GIS-AHP-Based Landslide Susceptibility Assessment of the Bradost Anticline, Northern Iraq

Ismaeel, O. A.,[1] Al-Jawadi, A. S.,[2] Adeeb, H. Gh. M.[3] and Thannoun, R. Gh.[4*]
[1]College of Education for Humanities, University of Mosul, Mosul, 00964, Iraq
[2]College of Petroleum and Mining Engineering, University of Mosul, Mosul, 00964, Iraq
[3]Dams and Water Resources Research Center, University of Mosul, Mosul, 00964, Iraq
[4]Remote Sensing Center, University of Mosul, Mosul, 00964, Iraq, E-mail: rayan.ghazi@uomosul.edu.iq
**Corresponding Author*

DOI: https://doi.org/10.52939/ijg.v22i10.5233

Abstract
The use of landslide susceptibility assessment is a vital step for sustainable land-use planning and risk mitigation, especially in mountainous areas and in complex tectonic and geomorphological environments. The present study aims to assess the landslide susceptibility in the Bradost Anticline through an integrated Geographic Information System (GIS) and Analytic Hierarchy Process (AHP) approach. The following 10 conditioning factors were considered: geology, lineament density, slope, elevation, stream density, gully density, slope curvature, topographic wetness index, normalized difference vegetation index, land use/land cover. All the factors were treated, standardized and visualised as thematic GIS layers. The AHP was then applied to normalize the weights, and the weighted layers were combined to create a landslide susceptibility map. Very high, high, and moderate stability zones cover 11.36%, 25.05%, and 29.87% of the area, respectively. The low and Very-low-stability areas constitute 23.05% and 10.67%, respectively, showing high or very high landslide susceptibility (33.72%) in the study area. The highest weights were recalculated for geology, lineament density, and slope (0.190, 0.188, and 0.179, respectively). An overall accuracy of 83.06%, a kappa coefficient of 0.787, and an area under the ROC curve of 0.894 were used to validate the model. These outcomes show a high level of agreement with the observations in the field and a high level of discriminatory performance. The framework can be used as a regional screening basis for landslide mitigation, land-use planning and infrastructure protection in vulnerable mountainous terrain.

Keywords: Bradost Anticline, GIS Development Tool, Rock Slope Stability Susceptibility, Spatial Modeling, Suitability Model

1. Introduction

In mountainous areas, steep slopes, weak or fractured rocks, erosion, hydrological processes, and human activities can create unstable conditions, leading to the potential occurrence of landslides, which can be one of the most damaging geological hazards. They can endanger lives, destroy settlements and infrastructure, impair transportation, and restrict sustainable land development. These impacts can be minimized by: (1) stabilizing individual slopes and (2) identifying slope areas that are naturally susceptible to failure early on. Landslide susceptibility is the relative spatiotemporal probability of occurrence of a landslide due to local terrain conditions, while landslide hazard also takes into account the spatiotemporal probability of occurrence of a landslide, and landslide risk encompasses the consequences of landslides on people, buildings, and infrastructure [1]. From field-based geologic and geotechnical investigations, landslide assessment has evolved to involve regional modelling with geographic information systems and remote sensing. GIS makes it possible to integrate geological, topographic, hydrological, environmental, land-use and landslide-inventory data across a large and geologically complex area [2]. The reliability of such susceptibility maps is, however, highly dependent on the quality of the landslide inventory, the relevance of the conditioning factors chosen, and the size and accuracy of the input data [3] and [4]. There are many landslide vulnerability modelling methodologies, and they can be broadly categorized as statistical, machine learning, or multi criteria decision making, most of the time analysis hierarchy process (AHP) is used as multi criteria decision making approach. With a large database of landslides and their controlling factors, statistical and

machine learning techniques can be used to reveal relationships between the two. Their effectiveness largely relies on the availability of accurate and complete landslide records and appropriate training and representation data [5] and [6]. Different, AHP offers a structured approach to incorporate expert knowledge and a multitude of environmental and geomorphological parameters by pairwise comparisons and the extraction of relative weights of the influencing parameters, which is suitable where valid and extensive historical landslide databases are not available [7] and [8]. Given the limited historical landslide inventory data in the study area, the GIS-AHP methodology was adopted as a suitable approach that combines the spatial analysis capabilities of Geographic Information Systems with the ability to represent the relative importance of the factors causing landslides in a systematic and interpretable manner. The available methods for mapping landslide susceptibility are generally divided into heuristic methods, statistical methods, physically based methods, and machine-learning methods.

To estimate relationships between past landslides and conditioning factors, statistical methods need to be employed, and a landslide inventory that is complete and representative enough. Physically based models offer a mechanical picture of the nature of the slope failure but must be applied on a regional scale and demand detailed spatial information about rock or soil strength, groundwater conditions, rock or soil thickness, and failure mechanisms. Models derived from machine-learning techniques can be used to model complex and non-linear relationships, and they can be highly predictive, but results are affected by the quality of the training data, sampling strategy, and model calibration, and some models remain difficult to interpret. Heuristic methods like the Analytic Hierarchy Process (AHP) are more open and can incorporate both numerical and categorical data, but their outcomes are also affected by expert judgments, factor classifications, and pairwise-comparison consistency. Therefore, there is no single best method; the specific method used should be tailored to the study goal, spatial scale, availability of data, data interpretability, and model validation [4] [6] and [9]. Comparative studies have demonstrated that AHP is not necessarily the most accurate prediction tool. AHP, frequency-ratio, bivariate statistical, weighting-factor, and logistic-regression models, for instance, have been found to differ in performance [10]. This emphasises that the results of AHP must be validated rather than assessed based on the spatial pattern of susceptibility classes, as validation is essential to ensure reliability. However, AHP can still be valuable in cases where geological information needs to be integrated with a mix of spatial data sources within a transparent and traceable system. It makes each conditioning factor appear important and provides a consistency test for determining contradictory judgments [11].

AHP was chosen as a regional screening and decision-making tool rather than assuming it is more accurate than other screening methods. It is suitable for the Bradost anticline because the analysis will involve a wide and complex area that needs to be integrated with geology, geomorphology, hydrology, environment, and land use. The approach also creates an understandable model that can be considered and examined by planners and infrastructure regulators. To minimize the subjective influence, factor weights are correlated with the geologic and geomorphologic conditions of the study area, the consistency of the pairwise comparisons is analyzed, and the final susceptibility map is tested using overall accuracy, the Kappa coefficient, and area under the receiver operating characteristic curve. The folded geological structures, steep rock slopes, and road construction are particularly favourable to slope instability in the mountainous terrain of northern Iraq. GIS and AHP were used in other parts of Iraq to integrate slope and geology, elevation, aspect, distances from faults, and drainage networks in landslide-susceptibility mapping [12]. Although useful and informative for the importance of geographical structures and for the assessment based on GIS, these studies do not allow for a spatially continuous evaluation of susceptibility throughout the Bradost anticline and surrounding populated areas. To fill this gap, the primary conditioning factors, such as the geological, geomorphological, hydrological, environmental, and land-use factors, were integrated into a GIS-based AHP model in the present study. The factors are normalized, weighted using pairwise comparisons, and aggregated to form an anticline-scale landslide susceptibility map. The study will go beyond evaluating each road cut and slope site to validate the resulting model, making it a very practical tool for identifying potentially unstable terrain, reviewing land-use proposals, planning residential and tourism development, and enhancing the safety of road infrastructure.

2. Methodology

This section describes the methodological framework adopted to assess landslide susceptibility across the Bradost anticline. It begins with a description of the study area and its main geographical and geological setting, followed by the preparation, weighting, integration, and validation of the selected conditioning factors within the GIS-based AHP model.

2.1 Geographical and Geological Setting

The Bradost anticline extends approximately 50 km, and two main roads run along its sides. Villages, sub-districts, and orchards are scattered along its sides (Figure 1). The Bradost anticline is situated in the Kurdistan Region of Iraq in the Imbricated Zone of the northwestern Zagros Fold–Thrust Belt [13]. The structure is a doubly plunging, doubly asymmetric, NW–SE-trending anticline, and is about 55 km long and 6–9.5 km wide. The southeastern end is in contact with the Korek and Handrin anticlines, while the northwestern end approaches the Shirin anticline close to the Barzan area [14] and [15]. The structural geometry of the anticline changes along strike and should not be shown as a single set of dip values along the entire length of the anticline.

The southwestern forelimb in the Shanidar sector is reported to dip at ~70°, while the northeastern backlimb is much flatter, with dips up to ~12° [16]. Based on the structural investigations, the Bradost structure is divided into segments where different styles of deformation occur – thrust-related and fault-controlled which explains the localization of the very steep bedding only in part of the anticline and not uniformly along the entire length [14]. This is asymmetrical and has direct consequences on slope stability. High bedding dips, fracturing due to thrusting, and road excavations on the steep southwest forelimb can form a slope with a bedding plane or other discontinuities, with outcrops on the slope face, enhancing the risk of planar or wedge failure. Instability can also be expected on the less steep northeast side, where bedding is roughly parallel to the ground surface, especially if supported by erosion, water infiltration, or excavation. Thus, the stability response of each limb will also be influenced by the relationship between bedding orientation, aspect of slope, joints, faults, and the geometry of engineered cuts, as well as the magnitude of dip. Competent limestone and dolostone of the Qamchuqa and Bekhme formations dominate the exposed succession, while weaker marl, shale, sandstone, and claystone units make up the bulk of the exposed succession and are primarily from the Sarmord, Balambo, Shiranish, and Tanjero formations (Figure 2). There are mechanical contrasts between the massive carbonate rocks and the weaker fine-grained layers, which enhance differential weathering and could localise deformation or failure along bedding contacts.

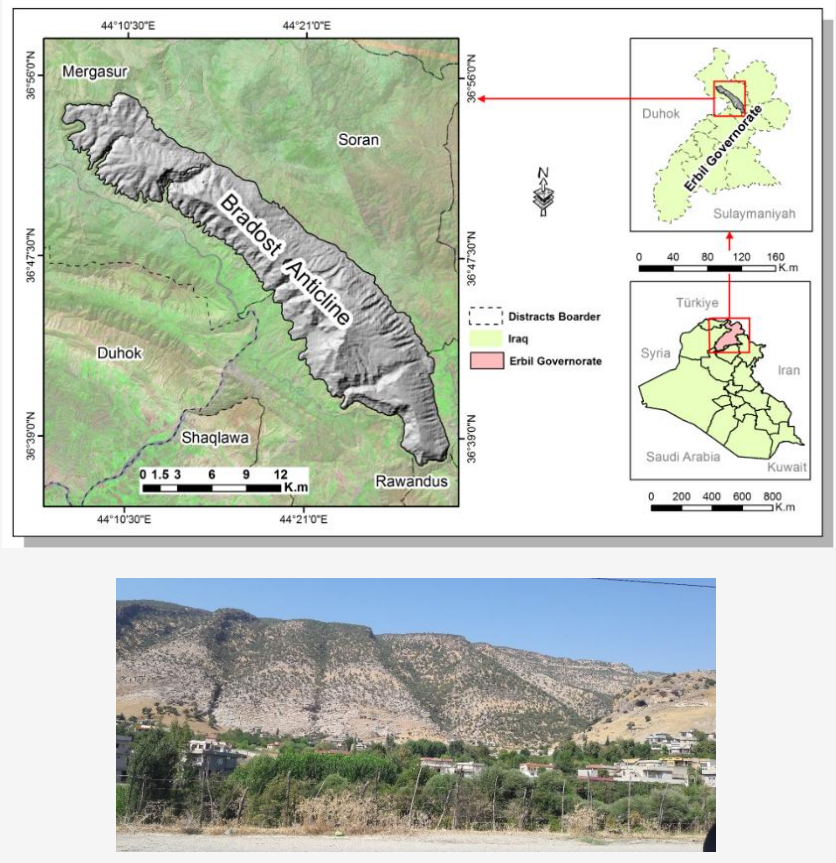


Figure 1: Geographic location of the Bradost Anticline in northern Iraq, with a field view of its southwestern limb

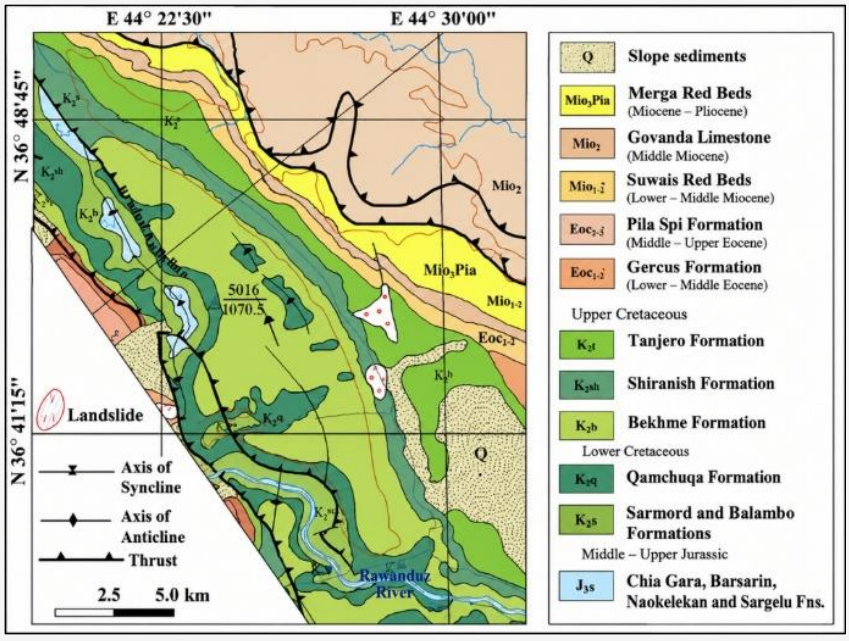


Figure 2: Geological map of the Bradost Anticline (modified from [17])

2.2 Methodology Procedure

The methodology was applied *in* a series of well-defined steps. A wide range of potential landslide-conditioning factors has been assembled from previous geological, geomorphological, geotechnical, and GIS-based susceptibility studies. The selection of factors was not only guided by the frequency of occurrence of the factors in the literature, but also by the relevance of the factors found in the literature to slope instability, applicability to the specific geological and environmental conditions of the Bradost anticline, and availability of quality data, spatial resolution, and regional coverage. Where there was no reliable and continuous data at the regional level, these factors were not included. The other candidate factors were then assessed for conceptual overlap and statistical redundancy, and only factors that allowed for distinct and interpretable information were included in the final model. Therefore, the selected factors balance scientific relevance, data availability, model scale compatibility, and suitability for regional landslide-susceptibility assessment. Similar studies on Slope Stability susceptibility found the most recurrent factors [18][19][20][21][22][23][24][25][26][27][28][29][30] and [31]. Reclassifying the layers according to the scientific literature for each element affecting ground Slope Stability susceptibility was the second stage of modeling the influencing factors to create a map of ground Slope Stability susceptibility in the research area (Figure 3).

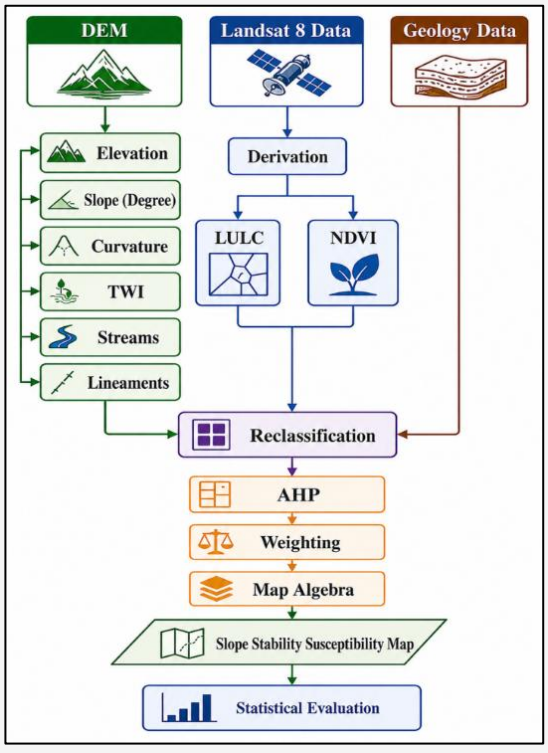


Figure 3: Landslide susceptibility assessment

The study used data from multiple sources to assess slope stability (Table 1). The Landsat 8 OLI Collection 2 Level-2 surface-reflectance scene LC08_L2SP_169034_20250312_20250324_02_T1_SR, acquired on 12 March 2025, was selected because it covers the entire Bradost Anticline and has

4.68% scene cloud cover. March falls within the wet season in northern Iraq and provides strong seasonal vegetation expression while retaining adequate cloud-free coverage; therefore, the NDVI layer represents wet-season conditions rather than a long-term vegetation climatology. The USGS Level-2 product already contains radiometric calibration, atmospheric correction, and terrain correction; ENVI was used for QA-based cloud masking, application of the published surface-reflectance scale factor, image subsetting, and supervised land-use/land-cover classification. NDVI was calculated in ArcGIS Desktop from the red and near-infrared surface-reflectance bands. Lineaments were extracted in PCI Geomatics. All spatial layers were projected to WGS 1984 UTM Zone 38N and resampled to a common 30 m grid using nearest-neighbor resampling for categorical layers and bilinear resampling for continuous layers.

2.3 Influencing Factors

2.3.1 Geology

The study area consists of the Chia Gara, Qamchuqa, Balambo, Aqra-Bekhme, Shiranish, and Bai Hassan formations and slope deposits. A geological map was imported into the GIS environment, and the boundaries of geological formations were digitized as polygon vector features with their lithological attributes given. The resulting vector layer was then converted to a raster layer, using a polygon-to-raster procedure, which assigned the code of each geological formation to each raster cell corresponding to that formation. The lithology was added as an important landslide conditioning factor because variations in rock strength, weathering resistance, bedding characteristics, and geological structure are directly related to slope mechanical behaviour. Competent rock units, meaning that they are relatively strong or have high weathering resistance, are less likely to become unstable than are rock units that are now weak or weathered [33] and [34].

2.3.2 Lineament density

The density of lineaments affects Slope Stability susceptibility through the formation of discontinuities, which favor shear failure [45]. The lineament density layer was derived from the lineament data extracted from the Digital Elevation Model (DEM). In this context, the digital elevation model (DEM) was obtained from Shuttle Radar Topography Mission (SRTM) data with a spatial resolution of 30 m from the USGS Earth Explorer platform. These data were used to derive several topographic variables, including elevation, slope, curvature, and topographic moisture index. The data were uploaded and processed in ArcGIS Desktop 10.8, consistent with the other spatial layers used in the study. The lineament data were initially mapped as a vector that was defined by the predominant structural and topographic characteristics of the study area, and then turned into a spatial density layer using the Kernel Density tool of ArcGIS 10.8 Desktop. To maintain the spatial consistency of the other layers used in analysis, a cell size of 30 m was selected. The search radius parameter was not specified because the software automatically calculates the radius based on the spatial distribution and density of the features to search for. This will provide a more accurate representation of the spatial pattern of the lineament data without reducing the objectivity of the results. Structural weaknesses in rocks are shown as lineaments, which can increase weathering and water permeability, thus decreasing shear strength and increasing the probability of landslides [35].

Table 1: Data sources, acquisition details, formats, and final raster resolution

Factor	Data format	Final raster resolution (m)	Type	Source
Geology	Vector	30	Map	[32]
NDVI	Raster	30	Landsat 8 OLI C2 L2 SR; 12 March 2025	USGS EarthExplorer (scene ID reported in text)
LULC	Raster	30	Landsat 8 OLI C2 L2 SR; 12 March 2025	USGS EarthExplorer (scene ID reported in text)
Elevation	Raster	30	DEM	https://dwtkns.com/srtm30m/
Slope	Raster	30	DEM	https://dwtkns.com/srtm30m/
Streams	Vector	30	DEM-derived drainage	SRTM 30 m DEM
Lineaments	Vector	30	Lineament extraction	PCI Geomatics and SRTM 30 m DEM
Gully Density	Raster	30	Mapped gully centerlines; normalized density	Shaded relief with Landsat cross-check
Curvature	Raster	30	DEM	https://dwtkns.com/srtm30m/
TWI	Raster	30	DEM	https://dwtkns.com/srtm30m/

6Table 2: Classification thresholds and susceptibility ratings of the conditioning factors

Factor	Unit	Class	Susceptibility Classification	Susceptibility Class Rating	References
Geology	Formation	Qamchuqa	Very low	1	[33] and [34]
		Aqra - Bekhme	Very low	1	
		Chia Gara	Low	2	
		Balambo	Low	2	
		Shiranish	Moderate	3	
		Bai Hassan	High	4	
		Slope Deposits	Very High	5	
Lineaments Density	m/km	0.05 - 0.36	Very low	1	[35]
		0.37 - 0.55	Low	2	
		0.56 - 0.74	Moderate	3	
		0.75 - 0.98	High	4	
		0.99 - 1.3	Very High	5	
Slope	Degree	0 - 15	Very low	1	[1]
		16 - 25	Low	2	
		26 - 35	Moderate	3	
		36 - 48	High	4	
		49 - 77	Very High	5	
Elevation	m	630 - 900	Very low	1	[36]
		910 - 1,100	Low	2	
		1,200 - 1,300	Moderate	3	
		1,400 - 1,500	High	4	
		1,600 - 2,100	Very High	5	
Stream Density	m/km	0.024 - 0.42	Very low	1	[37]
		0.43 - 0.68	Low	2	
		0.69 - 0.91	Moderate	3	
		0.92 - 1.2	High	4	
		1.3 - 1.6	Very High	5	
Gully Density	Normalized (0-1)	0.00-0.20	Very low	1	[60]
		>0.20-0.40	Low	2	
		>0.40-0.60	Moderate	3	
		>0.60-0.80	High	4	
		>0.80-1.00	Very High	5	
Curvature	Value	-21 - -3.4	Very low	1	[39]
		-3.3 - -1	Low	2	
		-0.9 - 0.57	Moderate	3	
		0.58 - 3	High	4	
		3.1 - 24	Very High	5	
TWI	Value	5.3 - 7.1	Very low	1	[40]
		7.2 - 8.4	Low	2	
		8.5 - 10	Moderate	3	
		11 - 12	High	4	
		13 - 20	Very High	5	
NDVI	Value	0.013 - 0.13	Very High	5	[41]
		0.14 - 0.18	High	4	
		0.19 - 0.23	Moderate	3	
		0.24 - 0.27	Low	2	
		0.28 - 0.51	Very low	1	
LULC	Class	Trees	Very low	1	[42]
		Crops	Moderate	3	
		Rangeland	Low	2	
		Built Area	High	4	
		Bare Ground	Very High	5	

2.3.3 Slope

Regarding the correlation between the slope angle and the geotechnical characteristics, including the angle of internal friction, the slope angle affects the Slope Stability susceptibility. The slope angle is also an important determinant of landslides because steeper slopes amplify the driving forces of gravity [1]. The slope layer was derived from the Digital Elevation Model (DEM) using the Slope tool in ArcGIS Desktop 10.8. This tool calculates the rate of

spatial change in elevation values between the central cell and its neighbors within a 3x3 cell analytical window, then determines the maximum rate of change to express the slope in degrees or percentage [46]. Slope is one of the most important factors affecting slope stability, as increasing the slope angle increases the effect of gravity on rock and sedimentary masses, thus increasing the likelihood of landslides and instability, particularly in areas with complex geological structures [47] and [48].

2.3.4 Elevation

The elevation factor influences the Slope Stability susceptibility by measuring the differences in elevation between neighbouring areas. The DEM was used to get the elevation layer. Geomorphological processes, such as erosion intensity and surface ruggedness, can be influenced by elevation and therefore possibly affect Slope Stability susceptibility [36].

2.3.5 Stream density

Land slope stability is influenced by stream density, and greater density correlates to greater risk. The morphology and drainage density of a catchment is significantly affected by hillslope processes [49]. A digital elevation model (DEM) was used to create the drainage network using hydrological analysis tools in ArcGIS Desktop 10.8. The process consisted of filling the depressions, determining the flow direction and flow accumulation, and finally extracting the drainage network from the area by using the flow accumulation value that is suitable for the study area. To achieve spatial uniformity with other layers used in the analysis, the drainage network was then converted to a stream density layer using the spatial analysis tools, with a cell size of 30 m. The density of streams is an important measure of topographic anatomy and surface runoff concentration, which are factors influencing slope stability and landslide susceptibility [37].

2.3.6 Gully Density

Gully density (*GD*) was used as a regional proxy for the concentration of mapped erosional incisions. Gully centerlines were digitized from the shaded-relief image and checked against the Landsat scene. Raw gully density is defined in Equation 1:

$$GD = \frac{\sum L_g}{A}$$

Equation 1

Where *GD* is gully density (km/km²), L_g is the length of each mapped gully segment (km), and A is the analysis area (km²). The continuous density raster was normalized using the min-max scaling method.

The normalized raster was classified into five explicit intervals using equal intervals. These dimensionless intervals correspond to susceptibility ratings 1-5, respectively. This density-based regional proxy does not estimate volumetric soil loss, which would require repeated field measurements of gully width, depth, and headcut retreat [60].

2.3.7 Curvature

Curvature is used to evaluate Slope Stability susceptibility by increasing the load for convex curvature and reducing it for concave curvature [50]. Concave curvature may lead to the appearance of daylight in the discontinuities on the slope surface. The curvature layer was derived from the Digital Elevation Model (DEM) using the Curvature tool within the Spatial Analyst toolkit in ArcGIS Desktop 10.8. This tool computes the rate of change in slope elevation and direction of surface orientation based on the elevation of adjacent cells, and distinguishes convex, concave, and flat surfaces. Curvature affects surface runoff patterns, moisture distribution, and material accumulation on slopes and is an important factor in determining slope stability and landslide potential. Slope curvature influences runoff distribution and water concentration; concave slopes accumulate water and sediment [39].

2.3.8 Topographic Wetness Index (TWI)

The Topographic Wetness Index (TWI) is the topographic potential for water accumulation and possible saturation. It was created from the hydrologically corrected DEM in ArcGIS Desktop 10.8, following the processing steps of Fill, Flow Direction, and Flow Accumulation [40]. TWI is expressed in Equation 2:

$$TWI = \ln \frac{A_s}{\tan \beta}$$

Equation 2

Where A_s is the specific catchment area per unit contour width is obtained from the flow accumulation and β is the local ground-slope gradient in radians.

A_s was determined as the number of 30 m cells contributing to a watershed multiplied by the cell area and divided by the contour width; and β was derived from the slope raster generated from the DEM, then converted from degrees to radians and passed into the tangent function in GIS.

The higher the TWI, the more likely the moisture is to accumulate and the lower the shear strength (with the caveats of a topography-based wetness proxy).

2.3.9 Normalized Difference Vegetation Index (NDVI)

The spatial effect of vegetation cover to control erosion and reinforce the root structure during the wet season was represented by the NDVI. It is computed from the surface-reflectance product of Landsat 8 Collection 2 on 12 March 2025. The month of March was chosen because it was within the rainy period in the North of Iraq, when the response of vegetation and the difference in soil moisture were well expressed; and the selected scene was characterized by only 4.68% cloud cover. A covariate derived from NDVI is hence a measure of the wet period of the season rather than a fixed property. The relatively low AHP adds little to the low sensitivity of the final index to short-term phenological variation. The NDVI is calculated from Equation 3:

$$NDVI = \frac{\rho NIR - \rho RED}{\rho NIR + \rho RED}$$

Equation 3

Where ρNIR is the scaled surface reflectance of Landsat 8 OLI Band 5, and ρRED is the scaled surface reflectance of Band 4. Higher NDVI values indicate denser vegetation and lower landslide susceptibility, whereas low NDVI values characterize exposed surfaces that are more susceptible to weathering and erosion.

2.3.10 Land Use and Land Cover (LULC)

LULC was produced by supervised maximum-likelihood classification of the surface-reflectance image from Landsat 8 using training data gathered in the field. To maintain physical consistency with NDVI, trees were given a susceptibility rating of Very low (1) due to the protection offered to the surface by deep root structure and canopy interception, rangeland was given a susceptibility rating of low (2) for protection of the surface, crops were given a susceptibility rating of moderate (3) due to shallow root zone and variable seasonal root zone, built-up land was given a susceptibility rating of high (4) where construction, road cutting or drainage alteration and slope are associated, and bare ground was given a susceptibility rating of Very high (5) because of the lack of root cohesion and direct exposure to rainfall and runoff [41] and [42]. No attempt was made to consider buildings on flat terrain as separate landslide triggers.

Land use/cover (LULC) factor is one of the auxiliary factors to indicate the characteristics of the surface cover, the extent of human interference, as well as vegetation cover in the study area. The impact of land use categories on slope stability varies depending on the prevailing topographic, geological, and hydrological conditions; therefore, no single category can be considered a direct cause of landslides in isolation from other factors. In this context, bare land may be associated with increased instability in areas with steep slopes and sparse vegetation cover, whereas this effect may be negligible in flat or low-slope areas.

2.4 Analytic Hierarchy Process, Group Aggregation, and Map Algebra

The recalculated principal-eigenvector weights are geology 0.190, lineament density 0.188, slope 0.179, elevation 0.107, stream density 0.104, gully density 0.079, TWI 0.056, curvature 0.053, NDVI 0.026, and LULC 0.018. The maximum eigenvalue is 10.462, yielding CI = 0.0514 and CR = 0.0345 (3.4% when rounded to one decimal place). Because CR is below 10%, the aggregated comparison matrix is acceptably consistent [43] and [44].

2.5 Map Algebra based on AHP

AHP comparisons used Saaty's 1-9 scale. Thirty experts in geomorphology, engineering geology, GIS, remote sensing, hydrology, and water-resources engineering completed reciprocal pairwise comparisons. All experts were assigned equal influence[61]. The AHP weights are determined from the AHP Online System at https://bpmsg.com/ahp/ahp-calc.php. The aggregated value for row i and column j in the pairwise comparison matrix is determined from Equation 4:

$$\bar{a}_{ij} = \left(\prod_{k=1}^{K} a_{ij}^{k} \right)^{1/k}$$

Equation 4

Where $\bar{a}_{ij}$ is the aggregated comparison between criteria i and j, $a_{ij}{}^{k}$ is expert judgment, and $K = 30$. The consistency ratio is defined in Equation 5:

$$CR = \frac{CI}{RI}$$

Equation 5

Where CR is the consistency ratio, CI is the consistency index, and RI is Saaty's random consistency index. RI = 1.49 was used for n = 10 [58].

Table 3: Pairwise-comparison matrix and AHP weights of the conditioning factors

Factor	(1)	(2)	(3)	(4)	(5)	(6)	(7)	(8)	(9)	(10)	Weight
(1) Geology	1	1	2	2	3	1	3	4	6	9	0.190
(2) Lineaments	1	1	1	3	2	2	3	4	7	9	0.188
(3) Slope	1/2	1	1	2	4	2	3	4	5	9	0.179
(4) Elevation	1/2	1/3	1/2	1	2	1	2	2	5	9	0.107
(5) Gully Density	1/3	1/2	1/4	1/2	1	1	2	2	3	5	0.079
(6) Stream Density	1	1/2	1/2	1	1	1	2	2	4	6	0.104
(7) Curvature	1/3	1/3	1/3	1/2	1/2	1/2	1	1/3	4	3	0.053
(8) TWI	1/4	1/4	1/4	1/2	1/2	1/2	3	1	2	2	0.056
(9) NDVI	1/6	1/7	1/5	1/5	1/3	1/4	1/4	1/2	1	2	0.026
(10) LULC	1/9	1/9	1/9	1/9	1/5	1/6	1/3	1/2	1/2	1	0.018
Consistency Ratio						**3.4%**					

Consistency index (CI) is a metric used to quantify the degree of inconsistency within a pairwise comparison matrix. It is defined in Equation 6:

$$CI = \frac{\lambda_{\max} - n}{n - 1}$$

Equation 6

Where λ_{max} is the principal eigenvalue of the reciprocal pairwise-comparison matrix, and n is the number of influencing factors.

Landslide susceptibility index (LHI) is determined from Equation 7:

$$LHI = \sum_{i=1}^{10} w_i r_i$$

Equation 7

Where w_i is the normalized AHP weight of factor i, r_i is its standardized rating from 1 to 5 (Table 2).

The pairwise comparison matrix and the AHP derived weights of the conditioning factors are presented in Table 3.

The normalized index was reclassified into explicit equal-width intervals to make the procedure reproducible. The equal intervals were chosen due to the range of the normalized index being fixed and because fixed thresholds allow for easy comparison and independent replication. Equation 7 was applied to the weighted overlay in ArcGIS Desktop 10.8. The susceptibility classes are the reverse of the final stability labels; a high LHI_n indicates low stability. This relationship is explicitly written so as not to confuse the terms susceptibility and stability.

2.5 Validation Data and LULC Accuracy Assessment

Supervised maximum-likelihood classification was used to prepare the LULC map. The independent accuracy assessment was conducted with 115 reference samples, of which 103 were correctly classified, thus obtaining an accuracy of 89.57% and Kappa = 0.821. This LULC assessment is based on a landslide-susceptibility model that has not been validated. A total of 124 locations for observation of the slopes were surveyed with geologists and located with a Garmin GPS receiver that has a 3-5 m nominal accuracy for model validation. The points were spread among the mapped stability zones and classified by a 5-level rubric: Very high stability - no fresh tension cracks, displaced material or rockfall evidence in the field; high stability - some weathering or isolated raveling without evidence of movement; moderate stability - open discontinuities, localized erosion, or small displaced blocks with no evidence of movement; low stability - recent small failures, undercutting, road deformation, or fresh tension cracks; and Very low stability - fresh or very recent movement, small failure scarps, displaced masses or repeated rockfall deposits. The assigned class was saved to the point attribute table and matched with the class at the same location in the raster class. The five-class confusion matrix and Figure 4 show severity classes in the attribute data and mapping locations, respectively.

2.6 Confusion Matrix

One of the most commonly used ways to test and check the performance and accuracy of classification models is the confusion matrix. It compares the model-predicted categories with the reference categories or actual observations, and can measure how well the classification results are in accordance with reality. This matrix is used to quantify a number of important accuracy indicators, including overall accuracy and the kappa coefficient.

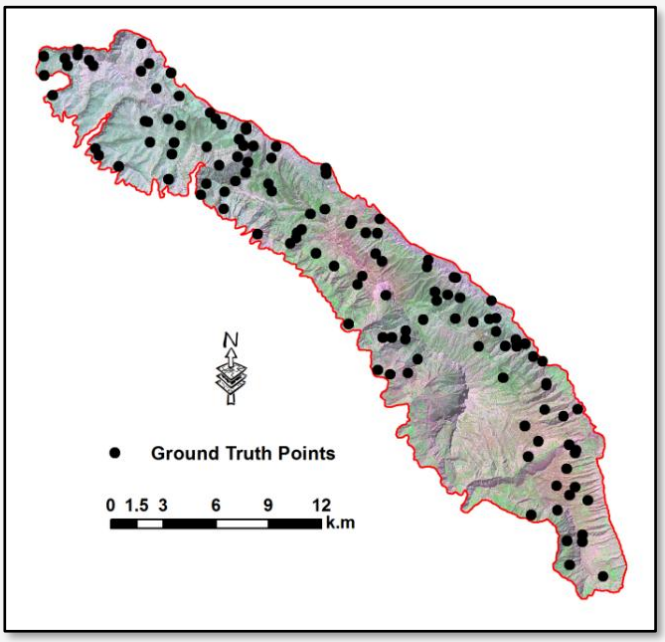


Figure 4: Locations of the 124 field-based slope-stability validation points

In this study, a confusion matrix was constructed by matching the model results with reference validation data. The resulting values were used to calculate overall accuracy as the ratio of correctly classified observations to the total number of observations. The kappa coefficient was used to estimate the degree of agreement between the model results and the reference data after excluding chance-induced agreement. This procedure is widely used to evaluate spatial and remote sensing models, as it provides an objective assessment of their reliability and accuracy [53] and [54].

2.7 ROC Curve and AUC

The five-class confusion matrix was used to assess exact class agreement. ROC analysis was performed separately with the continuous normalized susceptibility index (LHI_n). Field observations rated as low or very low stability were treated as positive unstable cases, whereas moderate, high, and very high stability observations were treated as negative cases. Using the continuous index rather than the five-class map permits threshold-independent evaluation [55] and [56]. The ROC curve relates the true-positive rate to the false-positive rate across all LHI_n thresholds. AUC values close to 1 indicate strong discrimination between unstable and comparatively stable field observations. This binary ROC analysis complements, rather than replaces, the ordinal five-class confusion matrix. The true-positive rate (TPR), false-positive rate (FPR), and area under the curve (AUC) were calculated using Equations 8-10:

$$TPR = \frac{TP}{TP + FN}$$

Equation 8

Where *TP* is the number of unstable field cases correctly ranked as positive, and *FN* is the number of unstable cases ranked as negative.

$$FPR = \frac{TP}{FP + TN}$$

Equation 9

Where *FP* is the number of comparatively stable cases ranked as positive, and T*N* is the number of stable cases ranked as negative.

$$AUC = \int_0^1 TPR(FPR)dFPR$$

Equation 10

Where *AUC* is the area under the receiver operating characteristic curve and *d(FPR)* represents the differential change in false-positive rate.

3. Results and Discussion

The spatial distribution of the ten conditioning factors shows clear geological, topographic, hydrological, and environmental contrasts across the Bradost Anticline (Figure 5). Resistant carbonate units dominate much of the structural core, whereas weaker formations and slope deposits occur mainly along the limbs.

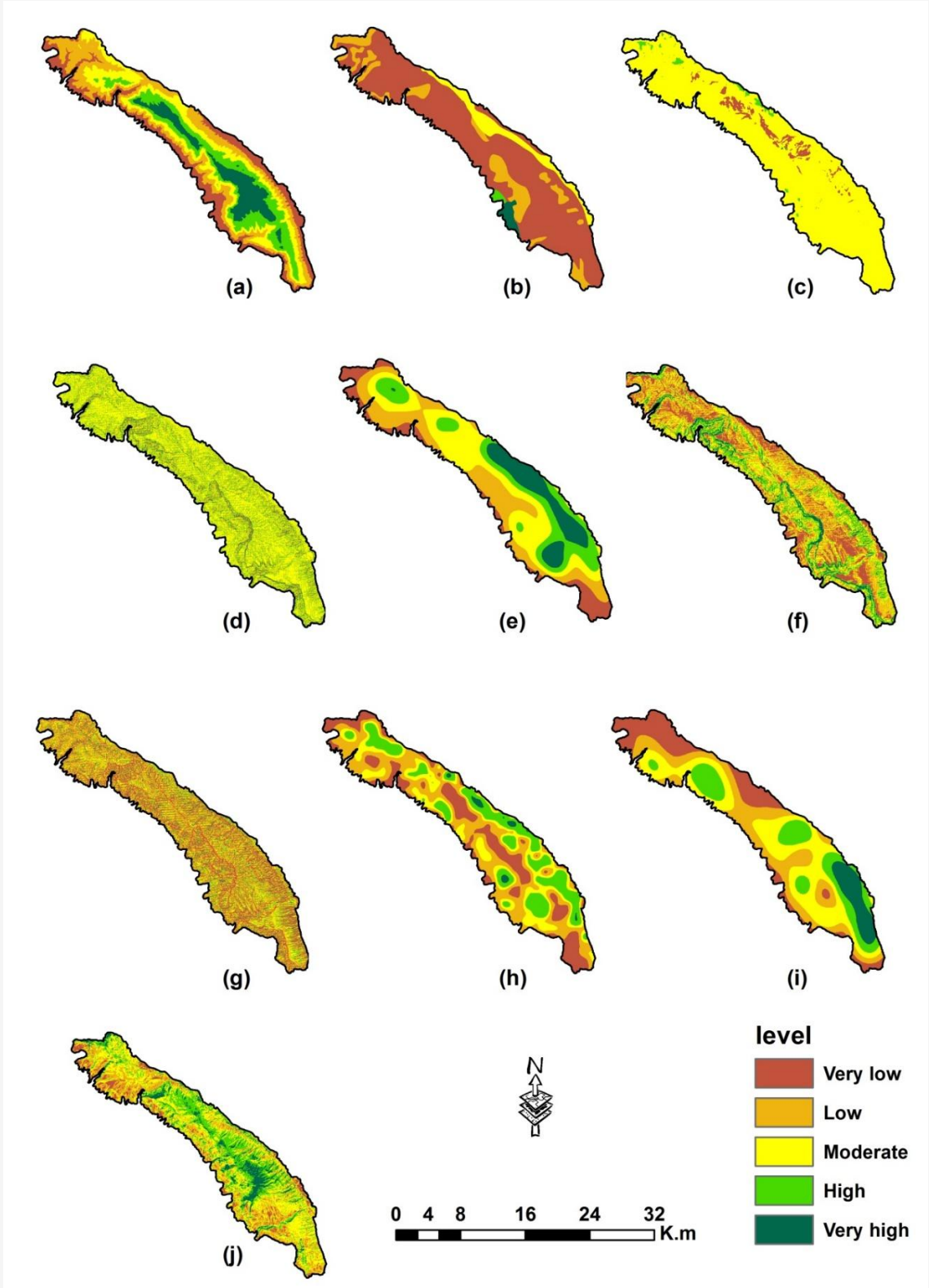


Figure 5: Landslide-conditioning susceptibility classes: (a) elevation, (b) geology, (c) LULC, (d) curvature, (e) stream density, (f) slope, (g) TWI, (h) normalized gully density, (i) lineament density, and (j) NDVI

The recalculated AHP weights identify geology (0.190), lineament density (0.188), and slope (0.179) as the three dominant controls, followed by elevation (0.107) and stream density (0.104). The final normalized index was classified using the fixed thresholds defined in Section 2.4 (Figure 6 and Table 4). The rockslide in the field is shown in Figure 7.

Table 4: The area and the percentage of each class of stability in the study area

Level	Area (km^2)	Percentage (%)
Very High Stability	30.76	11.36
High Stability	67.8	25.05
Moderate Stability	80.85	29.87
Low Stability	62.4	23.05
Very Low Stability	28.89	10.67
Sum	270.71	100.00

Very high- and high-stability zones occupy 11.36% and 25.05% of the area, moderate stability occupies 29.87%, and low- and Very-low-stability zones occupy 23.05% and 10.67%. Low-stability terrain is concentrated where steep slopes coincide with dense structural discontinuities, weaker lithology, and concentrated drainage. The corrected LULC ranking is physically consistent with NDVI: tree cover contributes the lowest susceptibility rating, whereas bare ground contributes the highest. Because NDVI and LULC have low weights (0.026 and 0.018), they refine local patterns but do not override the dominant. The confusion matrix showed that the model achieved an overall accuracy of 83.06%, reflecting a good ability to classify cases compared to the reference data. Confusion matrices and overall accuracy are common indicators of classification accuracy for spatial and sensory classifications [53] and [54]. The kappa coefficient was 0.787, indicating strong agreement between the model output and the reference data after excluding expected random agreement. According to the Landis and Koch scale, kappa values between 0.61 and 0.80 represent strong agreement, which enhances the model's reliability in representing the classified categories [59] (Table 5).

The validation results also showed that the Area Under the ROC Curve (AUC) was 0.894, indicating the model's high discriminatory ability across different categories. The result indicates that the model is highly efficient at correctly classifying sites compared to the reference data. The AUC achieves this when it approaches 1, which represents optimal model performance. According to the common classification of AUC values, those between 0.80 and 0.90 indicate excellent performance, while those above 0.90 indicate exceptional performance [55] and [56]. Therefore, the value achieved in this study confirms that the model possesses high predictive ability and good reliability in representing the spatial patterns of the studied phenomenon. It is also consistent with the confusion matrix, which showed an overall accuracy of 83.06% and a kappa coefficient of 0.787, thereby enhancing confidence in the model's outputs and its reliability for spatial analysis and decision support (Figure 8).

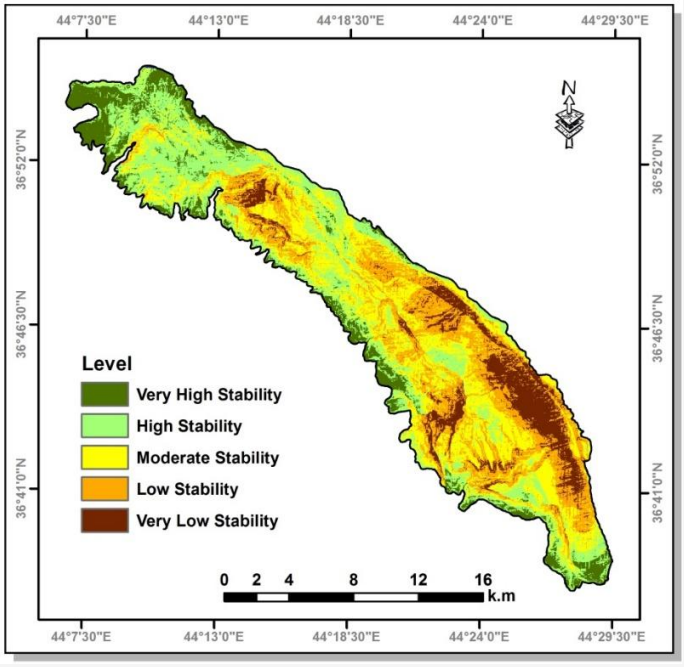


Figure 6: Landslide-stability classification of the Bradost Anticline derived from the normalized weighted susceptibility index

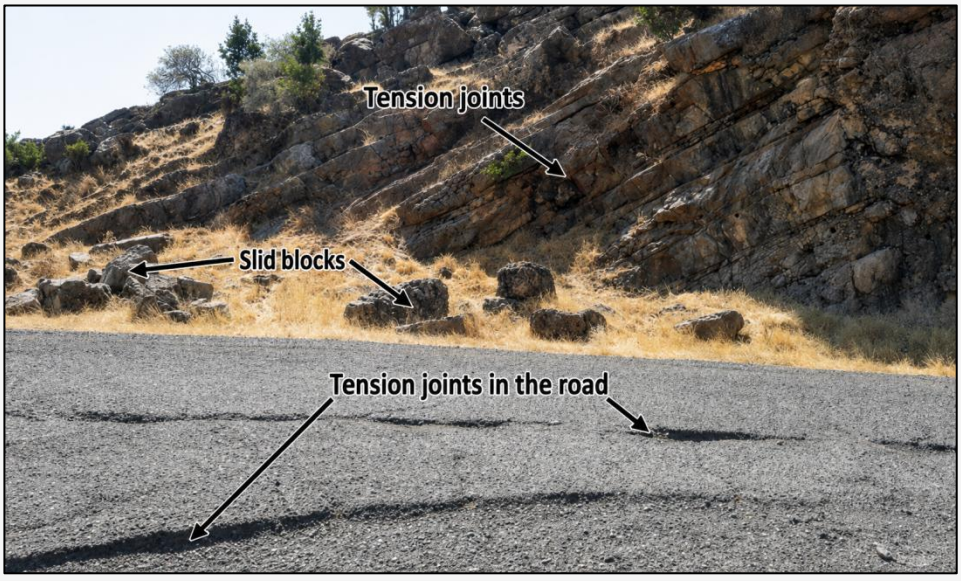


Figure 7: Field evidence of rock sliding and tension joints affecting the northeastern slope and adjacent road surface

Table 5: Confusion matrix between ground truth and the Slope Stability susceptibility model

Ground truth/Model	Very Low	Low	Moderate	High	Very High	Sum
Very Low	17	3	0	0	0	20
Low	1	24	2	0	0	27
Moderate	0	2	23	1	0	26
High	0	0	3	23	7	33
Very High	0	0	0	2	16	18
Sum	18	29	28	26	23	124

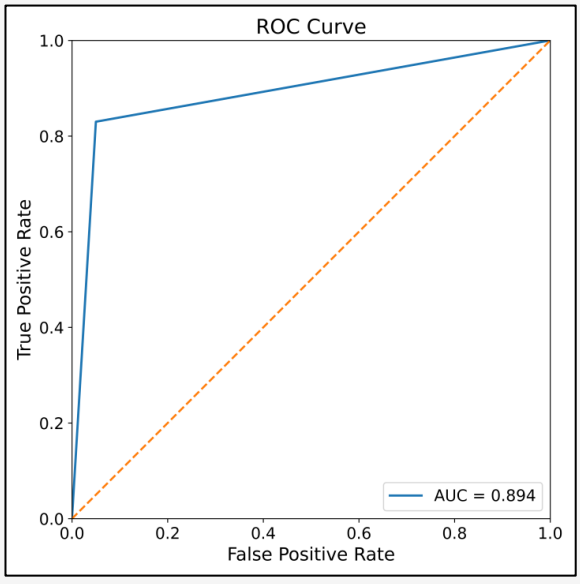


Figure 8: Receiver operating characteristic (ROC) curve for the continuous normalized susceptibility index

4. Conclusion

A regional GIS-AHP model was created to evaluate the susceptibility of landslides throughout the Bradost Anticline. Following the re-calculation of the reciprocal comparison matrix, geology (0.190), lineament density (0.188), and slope (0.179) are the main controls; their weights are similar but not the same. Secondary contributions are made by elevation (0.107), stream density (0.104), normalized gully density (0.079), and local spatial variation is provided by TWI, curvature, NDVI, and LULC. The corrected LULC scores are consistent with the mechanical features of vegetation and NDVI – trees are given the lowest susceptibility score and bare ground is given the highest. The last map shows 33.72% of the area as very low or low stability. The model was validated using 124 observations classified in the field, which yielded an overall accuracy of 83.06%, Kappa = 0.787, and AUC = 0.894, indicating that the model could be used as a regional screening tool. The map should not be used to perform a site specific engineering stability analysis since the rainfall time series, groundwater conditions, seismic loading, cohesion, friction angle, rock-mass rating, and pore-water pressure were not explicitly modeled. Repeated seasonal imagery, detailed gully measurement, field geotechnical data, and high-resolution elevation models should be incorporated into future work; temporally referenced landslide inventory.

References

[1] Dai, F. C., Lee, C. F. and Ngai, Y. Y., (2002). Landslide Risk Assessment and Management: An Overview. *Engineering Geology,* Vol. 64(1); 65-87. https://doi.org/10.1016/S0013-7952(01)00093-X.

[2] Thannoun, R. G., Al-Jawadi, A. S. and Adeeb, H. G. M., (2021). Three Dimensional Terrain Modeling for Tectonic Geomorphology of Chinara Anticline, Northern Iraq. *Iraqi Geological Journal,* Vol. 54(1), 53-65. https://doi.org/10.46717/igj.54.1C.5Ms-2021-03-25.

[3] Van Westen, C. J., Castellanos, E. and Kuriakose, S. L., (2008). Spatial Data for Landslide Susceptibility, Hazard, and Vulnerability Assessment: an Overview. *Engineering Geology,* Vol. 102(3–4); 112-131. https://doi.org/10.1016/j.enggeo.2008.03.010.

[4] Reichenbach, P., Rossi, M., Malamud, B. D., Mihir, M. and Guzzetti, F., (2018). A Review of Statistically-Based Landslide Susceptibility Models. *Earth-Science Reviews,* Vol. 180; 60-91. https://doi.org/10.1016/j.earscireVery2018.03.001.

[5] Pham, B. T., Pradhan, B., Bui, D. T., Prakash, I. and Dholakia, M. B., (2016). A Comparative Study of Different Machine Learning Methods for Landslide Susceptibility Assessment: A Case Study of Uttarakhand Area (India). *Environmental Modelling & Software,* Vol. 84, 240-250. https://doi.org/10.1016/j.envsoft.2016.07.005.

[6] Dao, M., Phan, T., and Nguyen, Q. (2026). Comparing Five Machine Learning Approaches for Local-Scale Landslide Susceptibility Mapping in the Huoi Reng Watershed, Central Vietnam. *International Journal of Geoinformatics*, Vol. 22(8), 23–41. https://doi.org/10.52939/ijg.v22i8.5139.

[7] Argyriou, A. VERY, Teeuw, R. M., Rust, D. and Sarris, A., (2015). GIS Multi-criteria Decision Analysis for Assessment and Mapping of Neotectonic Landscape Deformation: A Case Study from Crete. *Geomorphology,* Vol. 253; 262-274. https://doi.org/10.1016/j.geomorph.2015.10.01 8.

[8] Kayastha, P., Dhital, M. R. and De Smedt, F., (2013). Application of the Analytical Hierarchy Process (AHP) for Landslide Susceptibility Mapping: a Case Study from the Tinau Watershed, West Nepal. *Computers & Geosciences,* Vol. 52; 398-408. https://doi.org/10.1016/j.cageo.2012.10.003.

[9] Spiekermann, R. I., van Zadelhoff, F., Schindler, J., Smith, H., Phillips, C. and Schwarz, M., (2023). Comparing Physical and Statistical Landslide Susceptibility Models at the Scale of Individual Trees. *Geomorphology*, Vol. 440. https://doi.org/10.1016/j.geomorph.2023.108870.

[10] Khuc, T., Truong, X., Tran, V., Bui, D., Bui, D., Ha, H., Tran, T., Pham, T., and Yordanov, V. (2023). Comparison of Multi-Criteria Decision Making, Statistics, and Machine Learning Models for Landslide Susceptibility Mapping in Van Yen District, Yen Bai Province, Vietnam. *International Journal of Geoinformatics*, Vol. 19(7), 33–45. https://doi.org/10.52939/ijg.v19i7.2743.

[11] Komac, M., (2006). A Landslide Susceptibility Model using the Analytical Hierarchy Process Method and Multivariate Statistics in Perialpine Slovenia. Geomorphology, Vol. 74(1–4); 17-28. https://doi.org/10.1016/j.geomorph.2005.07.005

[12] Al-Dhahi, A. D., Hussain, A. I. and Al-Shwaily, A. K., (2023). Assessment of Landslide Susceptibility using the AHP and GIS Techniques for the Zurbatiya Region, East of Iraq. *Iraqi Geological Journal,* Vol. 56(2). https://doi.org/10.46717/igj.56.2D.16ms-2023-10-22.

[13] Omar, A. A., (2005). *An Integrated Structural and Tectonic Study of the Bina Bawi-Safin-Bradost Region in Iraqi Kurdistan.* Unpublished PhD Thesis, Department of Geology, Salahaddin University, Erbil, Iraq.

[14] Balaki, H. G. K. and Omar, A. A., (2019). Structural Assessment of the Bradost and Berat Structures in Imbricate and High Folded Zones-Iraqi Kurdistan Zagros Belt. *Arabian Journal of Geosciences,* Vol. 12(4). https://doi.org/10.1007/s12517-019-4251-1.

[15] Thannoun, R. G., Adeeb, H. G. M. and Al-Jawadi, A. S., (2022). Extractions Morphotectonic Features using Satellite Data Processing and Dem-derived Spatial Models. Iraqi Geological Journal, Vol. 55(1). 88-107. https://doi.org/10.46717/igj.55.1A.7Ms-2022-01-26.

[16] Sissakian, Very, K., Al-Ansari, N., Laue, J. and Abdulahad, D., (2022). Sinjar Anticline Northwest of Iraq: A Tectonic Geomorphological Study. *Proceedings of the 10th Annual International Forum on Water, Athens,* Greece; 11-14.

[17] Sissakian, Very, K. and Fouad, S. F., (2014). Geological Map of Sulaimaniyah Quadrangle, Scale 1:250,000. Iraq Geological Survey, Baghdad, Iraq. 151-161.

[18] Jeldes, I. A., Drumm, E. C. and Schwartz, J. S., (2013). The Low Compaction Grading Technique on Steep Reclaimed Slopes: Soil Characterization and Static Slope Stability. *Geotechnical and Geological Engineering,* Vol. 31(4), 1261-1274. https://doi.org/10.1007/s10706-013-9648-0.

[19] Sattler, T. and Paraskevopoulou, C., (2019). Implications on Characterizing the Extremely Weak Sherwood Sandstone: Case of Slope Stability Analysis using SRF at Two Oak Quarry in the UK. *Geotechnical and Geological Engineering,* Vol. 37(3); 1897-1918. https://doi.org/10.1007/s10706-018-0732-3.

[20] Aladejare, A. E. and Akeju, VERY O., (2020). Design and Sensitivity Analysis of Rock Slope using Monte Carlo Simulation. *Geotechnical and Geological Engineering,* Vol. 38(1); 573-585. https://doi.org/10.1007/s10706-019-01048-z.

[21] Al-Jawadi, A. S., (2021). Theoretical Models of Slope Stability Analysis in the Maqlub Mountain Rock Cut Routes, North Iraq. *Iraqi Geological Journal,* Vol. 54, 55-68. https://doi.org/10.46717/igj.54.1A.6Ms-2021-01-27.

[22] Zhang, G., Lu, G., Xia, C., Wu, L., Xu, Z., Bai, Y. and Li, J., (2022). A Sensitivity Analysis of the Anisotropy of Hydraulic Conductivity to the Seepage, Deformation and Stability of Anti-dipping Layered Rock Slopes: a Case Study of the Pulang Area in Southwestern China. *Geotechnical and Geological Engineering,* Vol. 40(1); 405-423.

[23] Al-Jawadi, A. S., Bety, A. K. S. and Ismaeel, O. A., (2022). Lineament Analysis by using Remote Sensing and GIS Technique of Sangaw Area, Kurdistan Region, NE Iraq. *Iraqi Geological Journal,* Vol. 55,152-163. https://doi.org/10.46717/igj.55.2C.11ms-2022-08-24.

[24] Thammaboribal, P., Triapthti, N., and Lipiloet, S. (2025). Using of Analytical Hierarchy Process (AHP) in Disaster Management: A Review of Flooding and Landslide Susceptibility Mapping. *International Journal of Geoinformatics*, Vol. 21(4), 177–196. https://doi.org/10.52939/ijg.v21i4.4091.

[25] Montoya-Araque, E. A. and Montoya-Noguera, S., (2023). Sensitivity Analysis of a Physically Based Model to Assess Rainfall-triggered Shallow Landslides. *Geotechnical and Geological Engineering,* Vol. 41(5); 2797-2814. https://doi.org/10.1007/s10706-023-02427-3.

[26] Arrasyid, R., Ruhimat, M., Ningrum, E., Ihsan, H., Setiawan, I., and Waluya, B. (2026). Assessment of Land Suitability and Spatial Development Direction for Hevea Brasiliensis Cultivation in West Bandung Regency, Indonesia. *International Journal of Geoinformatics*, Vol. 22(8), 128–150. https://doi.org/10.52939/ijg.v22i8.5144.

[27] Ali, R., Alnuaimy, Q., and Othman, A. (2026). High-Resolution Landslide Susceptibility Assessment along a Mountain Road Corridor in Carbonate Terrains Using Handheld SLAM LiDAR and GIS-Based AHP: Northeastern Iraq. *International Journal of Geoinformatics*, Vol. 22(9), 109–127. https://doi.org/10.52939/ijg.v22i9.5194.

[28] Al-Jawadi, A. S., (2024). Predicting Slip Surfaces for Slope Stability Assessment Along Highway 80 in Mosul, Northern Iraq. *Geotechnical and Geological Engineering,* Vol. 42(5); 2997-3008. https://doi.org/10.1007/s10706-023-02713-0.

[29] Nguyen, P. M. VERY and Marciniak, M., (2024). Stochastic Rock Slope Stability Analysis: Open Pit Case Study with Adjacent Block Caving. Geotechnical and Geological Engineering, Vol. 42(7). https://doi.org/10.1007/s10706-024-028 62-w.

[30] Al-Janqli, S. M. E. and Ismaeel, O. A., (2025). Spatial Modeling of Groundwater Potential Existence using GIS: Nineveh Governorate as a Model. *Iraqi National Journal of Earth Sciences,* Vol. 25(2); 38-56. https://doi.org/10.33899/earth.2024.146050.1217.

[31] Seeboonruang, U., Mandadi, R., Thammaboribal, P., Gonzales, A. L., Bharadwaz, G. S. V. S. A., (2025). Estimation of Soil Erosion and Enhancing Sediment Retention in the Lam Phra Phloeng Watershed: Insights from RUSLE and InVEST Modelling. *Water***.** Vol. 17. https://doi.org/10.3390/w17233339.

[32] Balaki, H. G. K. and Omar, A. A., (2019). Structural Assessment of the Bradost and Berat Structures in Imbricate and High Folded Zones-Iraqi Kurdistan Zagros Belt. *Arabian Journal of Geosciences,* Vol. 12. https://doi.org/10.1007/s12517-019-4251-1

[33] Varnes, D. J., (1978). Slope Movement Types and Processes. *Transportation Research Board Special Report,* Vol. 176, 11-33.

[34] Highland, L. M. and Bobrowsky, P., (2008). *The Landslide Handbook: A Guide to Understanding Landslides.* U.S. Geological Survey Circular 1325, Reston, Virginia, USA. https://pubs.usgs.gov/circ/1325/pdf/C1325_508.pdf.

[35] Lee, S. and Min, K., (2001). Statistical Analysis of Landslide Susceptibility at Yongin, Korea. Environmental Geology, Vol. 40(9), 1095-1113. https://doi.org/10.1007/s002540100310.

[36] Pradhan, B. and Lee, S., (2010). Delineation of Landslide Hazard Areas on Penang Island, Malaysia, by using Frequency Ratio, Logistic Regression, and Artificial Neural Network Models. *Environmental Earth Sciences,* Vol. 60(5); 1037-1054. https://doi.org/10.1007/s12665-009-0245-8.

[37] Montgomery, D. R. and Dietrich, W. E., (1994). A Physically Based Model for the Topographic Control on Shallow Landsliding. *Water Resources Research,* Vol. 30(4), 1153-1171. https://doi.org/10.1029/93WR02979.

[38] Morgan, R. P. C., (2005). *Soil Erosion and Conservation.* 3rd ed. Blackwell Publishing, Oxford, UK.

[39] Moore, I. D., Grayson, R. B. and Ladson, A. R., (1991). Digital Terrain Modelling: a Review of Hydrological, Geomorphological, and Biological Applications. *Hydrological Processes,* Vol. 5(1); 3-30. https://doi.org/10.1002/hyp.3360050103

[40] Beven, K. J. and Kirkby, M. J., (1979). A Physically-based Variable Contributing Area Model of Basin Hydrology. *Hydrological Sciences Bulletin,* Vol. 24(1), 43–69. https://doi.org/10.1080/02626667909491834.

[41] Glade, T., (2003). Landslide Occurrence as a Response to Land Use Change: a Review of Evidence from New Zealand. *Catena,* Vol. 51(3–4), 297-314. https://doi.org/10.1016/S0341-8162(02)00170-4.

[42] Crozier, M. J., (1986). *Landslides: Causes, Consequences and Environment.* Croom Helm, London, UK.

[43] Wind, Y. and Saaty, T. L., (1980). Marketing Applications of the Analytic Hierarchy Process. *Management Science,* Vol. 26(7); 641-658. https://doi.org/10.1287/mnsc.26.7.641.

[44] Malczewski, J., (1999). *GIS and Multicriteria Decision Analysis.* John Wiley & Sons, New York, USA.

[45] Ramli, M. F., Yusof, N., Yusoff, M. K., Juahir, H. and Shafri, H. Z. M., (2010). Lineament Mapping and its Application in Landslide Hazard Assessment: a Review. *Bulletin of Engineering Geology and the Environment,* Vol. 69(2); 215-233. https://doi.org/10.1007/s10064-009-0255-5.

[46] Burrough, P. A., McDonnell, R. A. and Lloyd, C. D., (2015). *Principles of Geographical Information Systems.* Oxford University Press, Oxford, UK.

[47] Ayalew, L. and Yamagishi, H., (2005). The Application of GIS-based Logistic Regression for Landslide Susceptibility Mapping in the Kakuda-Yahiko Mountains, Central Japan. *Geomorphology,* Vol. 65(1–2); 15-31. https://doi.org/10.1016/j.geomorph.2004.06.010.

[48] Pourghasemi, H. R., Pradhan, B. and Gokceoglu, C., (2012). Application of Fuzzy Logic and Analytical Hierarchy Process (AHP) to Landslide Susceptibility Mapping at Haraz Watershed, Iran. *Natural Hazards,* Vol. 63(2); 965-996. https://doi.org/10.1007/s11069-012-0219-2.

[49] Tucker, G. E. and Bras, R. L., (1998). Hillslope Processes, Drainage Density, and Landscape Morphology. *Water Resources Research,* Vol. 34(10); 2751-2764. https://doi.org/10.1029/98WR01474.

[50] He, L., Coggan, J., Francioni, M. and Eyre, M., (2021). Maximizing Impacts of Remote Sensing Surveys in Slope Stability-a Novel Method to Incorporate Discontinuities into Machine Learning Landslide Prediction. *ISPRS International Journal of Geo-Information,* Vol. 10(4). https://doi.org/10.3390/ijgi10040232

[51] Thannoun, R. G. and Ismaeel, O. A., (2024). Flood Risk Vulnerability Detection Based on the Developing Topographic Wetness Index Tool in Geographic Information System. *IOP Conference Series: Earth and Environmental Science,* Vol. 1300(1). https://doi.org/10.1088/1755-1315/1300/1/012012.

[52] Khalil, A., Abdullah, O. A. I. and Kareem, A. T., (2024). GIS Application for Creating Potential Flood Map using AHP: a Case Study in Chaq-Chaq Valley, Sulaymaniyah City, Kurdistan Region, Iraq. *Iraqi Geological Journal,* Vol. 57, 254-263. https://doi.org/10.46717/igj.57.2C.17ms-2024-9-25.

[53] Congalton, R. G. and Green, K., (2019). *Assessing the Accuracy of Remotely Sensed Data: Principles and Practices.* CRC Press, Boca Raton, Florida, USA.

[54] Foody, G. M., (2002). Status of Land Cover Classification Accuracy Assessment. *Remote Sensing of Environment,* Vol. 80(1); 185-201. https://doi.org/10.1016/S0034-4257(01)00295-4.

[55] Swets, J. A., (1988). Measuring the Accuracy of Diagnostic Systems. *Science,* Vol. 240(4857), 1285-1293. https://doi.org/10.1126/science.3287615.

[56] Fawcett, T., (2006). An Introduction to ROC Analysis. *Pattern Recognition Letters,* Vol. 27(8); 861-874. https://doi.org/10.1016/j.patrec.2005.10.010.

[57] Saaty, T. L., (2003). Decision-making with the AHP: Why Is the Principal Eigenvector Necessary. *European Journal of Operational Research,* Vol. 145(1); 85-91. https://doi.org/10.1016/S0377-2217(02)00227-8.

[58] Saaty, T. L., (2008). Decision Making with the Analytic Hierarchy Process. *International Journal of Services Sciences,* Vol. 1(1); 83-98. https://doi.org/10.1504/IJSSCI.2008.017590.

[59] Landis, J. R. and Koch, G. G., (1977). The Measurement of Observer Agreement for Categorical Data. *Biometrics,* 159-174. https://doi.org/10.2307/2529310.

[60] Nhu, VERY H., Janizadeh, S., Avand, M., Chen, W., Farzin, M., Omidvar, E., Shirzadi, A., Bui, D. T. and Pourghasemi, H. R., (2020). GIS-Based Gully Erosion Susceptibility Mapping: A Comparison of Computational Ensemble Data Mining Models. *Applied Sciences.* Vol. 10(6). https://doi.org/10.3390/app10062039.

[61] Forman, E. H. and Peniwati, K., (1998). Aggregating Individual Judgments and Priorities with the Analytic Hierarchy Process. *European Journal of Operational Research,* Vol. 108(1); 165-169. https://doi.org/10.1016/S0377-2217(97)00244-0.